Single-crystalline hexagonal ZnO microtube optical resonators†

Hongxing Dong,[a] Zhanghai Chen,*[a] Liaoxin Sun,[a] Wei Xie,[a] H. Hoe Tan,[b] Jian Lu,[a] Chennupati Jagadish[b] and Xuechu Shen[a]

Received 27th January 2010, Accepted 13th April 2010
First published as an Advance Article on the web 2nd June 2010
DOI: 10.1039/c0jm00172d

High quality ZnO microtubes with hexagonal cross sections, fabricated *via* an oxidation–sublimation process, are studied as novel optical resonators. Whispering gallery modes, Fabry-Pérot modes, and an additional set of modes with different polarizations are directly observed in the visible spectral range at room temperature by using the spatially resolved spectroscopic technique. The diameter and wall thickness of the microtube are crucial for light modulation. The experimental results are explained and fitted with a plane wave interference model and Cauchy dispersion formula for refractive indices.

Introduction

Semiconductor microcavities are of great importance for developing optoelectronic devices owing to their microscopic size, high quality factor Q, and low lasing threshold power.[1–3] In a semiconductor resonator, the propagation of light in all three dimensions can be confined and modulated, which allows precise control of the electromagnetic field and the photon density of states in a prescribed manner. This precise manipulation of light–matter interaction is essential for both fundamental physics research in the field of cavity quantum electrodynamics and the development of miniature optoelectronic devices including lasers,[4] optical waveguides,[5] tunable filters,[6] and optical sensors *etc*.[7] Recently, micro/nanostructures with hexagonal cross section have drawn considerable interest for optical resonator applications due to their unique, well-defined geometry and excellent optical properties. However, so far, practical examples of semiconductor micro/nanostructures in the form of hexagonal whispering gallery mode (WGM) resonators are very rare. To the best of our knowledge, except for nanowires and nanonails of ZnO and In_2O_3,[8–10] the synthesis of high quality hexagonal cavities remains very difficult; therefore, an imperative and challenging issue is to develop new and efficient hexagonal resonators. One dimensional tubular structures are important building blocks for nanoscale devices owing to their unique structural characteristics.[11–13] It is believed that if the tubular structures with hexagonal cross section can function as optical cavities, the optical modulation will be affected by the inner surfaces of the microtubes and their optical properties will be more complex than those of single wall microcavities. Furthermore, since one can fill the tubular cavities with luminescent materials, they are expected to have great potential for new applications such as novel multicolor lasers.

ZnO is, so far, one of the most widely used and highly efficient optoelectronic materials for UV or visible photonic devices because of its wide bandgap (~3.37 eV) and large exciton binding energy (~60 meV). Numerous ZnO nanostructures with different morphologies,[14–18] including the highly desirable tubular structures, have been demonstrated. However, the synthesis of three-dimensional tubular structure of ZnO remains challenging compared with other materials that have bulk lamellar structures, such as graphite or graphite-like structures. Only a few methods, such as vapor-phase reaction,[19,20] template-assisted growth[21] and wet chemical methods,[22,23] have been employed so far. Most of the synthesized micro/nanotubes have either irregular circular cross sections or poor crystal quality with rough surfaces. Although hexagonal ZnO micro/nanotube arrays have been demonstrated, an isolated, undamaged, single-crystalline ZnO tube from the arrays is difficult to obtain. Therefore, the application of a single ZnO micro/nanotube as an optical cavity has not yet been explored.

In this work, we report the synthesis and the optical properties of free-standing, high quality ZnO microtubes with hexagonal cross sections that can be used as optical resonators. These microtubes were directly formed through a simple oxidation–sublimation process. Compared with the methods mentioned earlier, our approach does not require catalysts, templates, carrier gases, or low pressure. WGMs, Fabry-Pérot modes (FPMs) and wave-guided modes with different polarization (TE, E$\perp c$-axis and TM, E$\|c$-axis) were directly observed in the visible spectral range at room temperature, and the modulation was mapped directly by using the spatially resolved spectroscopic technique. The resonator properties in relation to the tube cavity diameter and wall thickness were studied in detail. Calculations based on the plane wave interference model and Cauchy dispersion functions agree well with the experimental data. The experiments and theoretical analyses indicate that the ZnO hexagonal microtube resonator is a promising test-bed for investigating new optical modulation behavior and developing novel optical devices.

Experimental

The growth of the ZnO microtubes was carried out in a horizontal tube furnace. No catalysts, carrier gases, low pressure, or

[a]*Surface Physics Laboratory, Department of Physics, Advanced Materials Laboratory, Fudan University, Shanghai 200433, China. E-mail: zhanghai@fudan.edu.cn*
[b]*Department of Electronic Materials Engineering, Research School of Physics and Engineering, The Australian National University, Canberra, ACT 0200, Australia*

† Electronic supplementary information (ESI) available: SEM images of ZnO nanowires and microtubes. See DOI: 10.1039/c0jm00172d

templates were used in the experiment. In a typical experimental procedure, a mixture of ZnO powders and graphite powders with a weight ratio of 1 : 1 was loaded into a small quartz boat. A clean Si wafer was covered over the top of the boat, and then the boat was placed in the center of the quartz tube. The ends of the quartz tube were sealed by using flexible plastic switches that ensured the appropriate pressure formed in the quartz tube during the heating process. This quartz tube was then placed at the center of the horizontal tube furnace. The oxygen source came from the air present in the quartz tube. The temperature of the tube furnace was raised to 1000 °C at a rate of 25 °C min^{-1} and the temperature was maintained at 1000 °C for 60 min. After the furnace was cooled to room temperature, a large amount of crystal-like product was found in the quartz boat where the raw materials were located. The morphologies, structures and composition of the products were characterized by scanning electron microscopy (SEM, JEOL 6400), transmission electron microscopy (TEM, JEOL 2010), energy-dispersive X-ray spectroscopy (EDS), X-ray diffraction (XRD, D/max-rB diffractometer with Cu Ka radiation ($\lambda = 1.54$ Å) at scanning speed of 8° min^{-1} in the range of 30–70°). Optical studies of individual ZnO microtubes were carried out using a confocal micro-photoluminescence system, with the He–Cd laser line of 325 nm as the excitation source. The excitation laser was focused onto the microtube with a spot size of ~1 μm in diameter by a microscope objective (40×) and scanned at steps of 0.5 μm along the *c*-axis of the ZnO microtube. Polarization-resolved μ-PL was performed with TE and TM configurations. The electrical vector of excitation laser *E* was always parallel to the *c*-axis. All of the PL data were recorded using a silicon CCD detector through 600 lines/mm grating.

Results and discussion

Fig. 1(a) exhibits a typical SEM image of the ZnO microtubes. It can be seen that the ZnO microtubes with conical tip were grown with a high yield. The ZnO microtubes have lengths in the range of 100–300 μm with a diameter continuously decreasing from 5–20 μm at the tip to several micrometres at the root. Some microtubes with uniform size are also observed. Fig. 1(b) and (c) show the side and top views, respectively, of a single ZnO microtube, revealing that the microtubes have a highly regular hexagonal cross section and smooth inner and outer surfaces. The TEM image further reveals that the ZnO microtubes have very uniform morphology and smooth surfaces with conical tips. High resolution TEM image taken from the rectangular region marked in Fig. 1(d) clearly displays the resolved lattice fringes of 0.26 nm, which corresponds to the (0002) planes of the wurtzite ZnO structure (Fig. 1(e)). The corresponding selected area electron diffraction (SAED) pattern shown in the inset of Fig. 1(e) illustrates the microtube to be single crystal. The XRD patterns of the samples are shown in Fig. 1(f). The diffraction peaks can be indexed as hexagonal wurtzite-type ZnO (JCPDS No.65-3411). An enlarged view of the diffraction peaks between 35° and 45° is shown in the inset of Fig. 1(f). Very weak Zn (002), (100) and (101) diffraction peaks were observed (JCPDS No.65-3358). The signals are from the unoxidized Zn formed during the synthesis process due to insufficient oxygen in the system. Fig. 2(a) is a SEM image of a typical ZnO microtube dispersed onto a silicon substrate. With the elemental mapping analysis shown in Fig. 2(b) and (c), the EDS data confirmed the uniform distribution of Zn and O elements across the

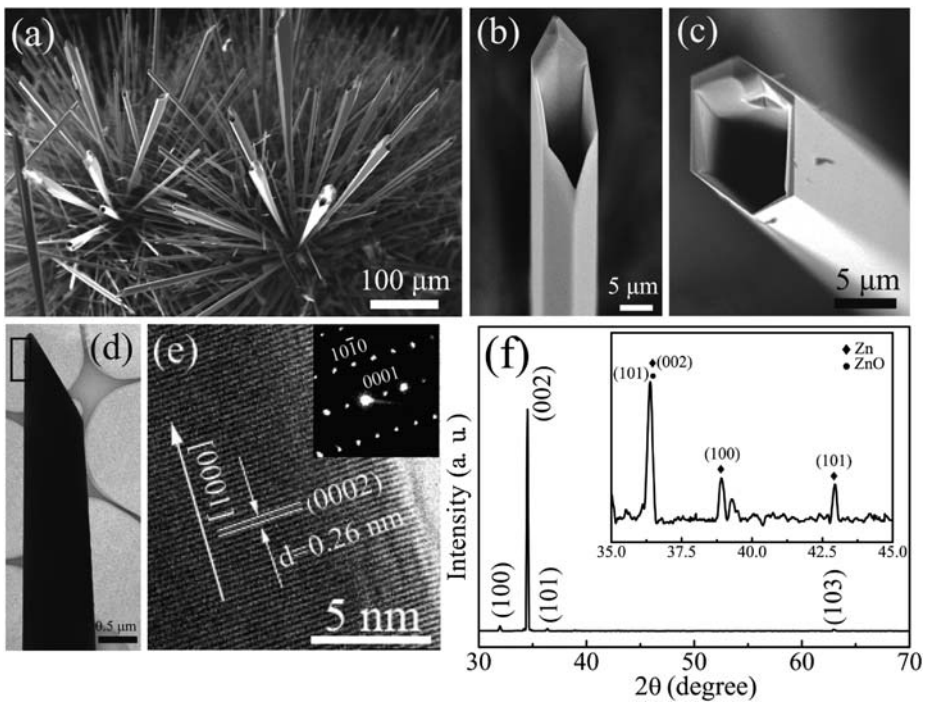

Fig. 1 (a–c) SEM images of the microtubes at different angles and magnifications, (d) TEM image of a single microtube, and (e) HRTEM image and the corresponding SAED pattern (inset) from the rectangular region marked in (d). (f) XRD pattern of ZnO microtubes. The inset is an enlarged view of the diffraction peaks between 35° and 45° showing the presence of Zn.

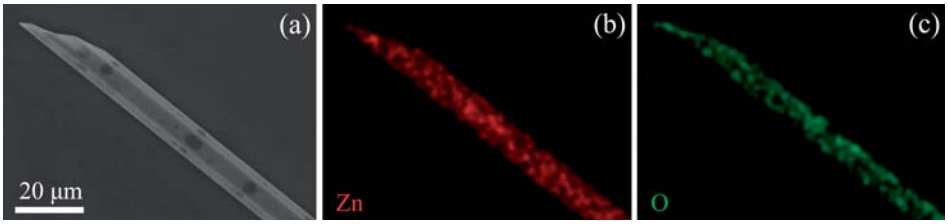

Fig. 2 (a) SEM image of a typical ZnO microtube. (b) and (c) EDS elemental mappings of Zn and O, respectively.

microtube. It was noticed that the element Zn was abundant in the microtube, which is in agreement with the above XRD results.

The formation of the ZnO microtubes is believed to be governed by a simple oxidation–sublimation process. In our system, graphite acts as a reducing agent, resulting in ZnO powder being reduced to Zn vapor at high temperature. With the increase of the concentration of the Zn vapor, Zn atoms condense and form liquid clusters in the quartz boat. At the same time, the liquid clusters reoxidize in the oxygen environment, forming Zn/ZnOx ($x < 1$) nanostructures at the nucleation sites. Both Zn and ZnO belong to the hexagonal crystal system, and they all have three fast growth directions along [0001], [10$\bar{1}$0], and [2$\bar{1}\bar{1}$0]. These unique structural properties are conducive to the formation of nanorods with hexagonal cross section. Once formed, the nucleus rod will react with the oxygen from the environment to form ZnO. The Zn {0001} surfaces have lower energy than the {10$\bar{1}$0}/{2$\bar{1}\bar{1}$0} surfaces, which tend to be the most stable and least resistant to oxidation.[24] Therefore, the sidewall of a hexagonal nanorod is oxidized into ZnO, which eventually form the shell. At the same time, the remaining Zn inside the nanorods is sublimed through the tips at the {0001} surface because of the low melting point of Zn (419.5 °C), leading to the formation of hexagonal ZnO microtubes. The morphology of the conical tip may be controlled by the kinetics during this unique reduction–oxidation process.[25] It is noticed that insufficient oxygen is crucial for the formation of the tube-like microstuctures. In fact, ZnO nanowires instead of tubular structures were obtained if the ends of the quartz tube were not sealed during the growth process (Fig. S1, ESI†).

Fig. 3(a) and (b) show the SEM images of a typical single perfect and cracked ZnO microtube, respectively. One can see that the inner and outer surfaces of the microtube are flat and smooth hexagonal facets. Usually, two possible resonant cavity modes, WGMs and FPMs, can be formed in this kind of microstructure as shown in Fig. 3(c) and (d), respectively. For WGMs, a light wave confined within the hexagonal cross section is supposed to circulate inside the microtube wall as indicated by the white arrows. Due to the large refractive index of ZnO ($n \approx 2.0$) in the visible spectral range, multiple total internal reflections (TIRs) in the hexagonal microcavity were easily achieved.[1] According to the plane wave model,[26] if the wall thickness, d, and the outer diameter, R, satisfy the relationship $d \geq \sqrt{3}R/8$, then light waves can circle around due to TIRs at the interface between the ZnO microtube walls and air, hence forming a WGM. The flat and smooth surface morphology and wall thickness are crucial for high quality waveguides without large losses from the surfaces, thereby leading to a high quality factor and low lasing threshold of the cavity. For FPMs, the light wave travels back and forth between two opposing interfaces of the microtube wall. Taking into account the number of TIRs and path length for each resonance mode, we obtained the following mode equations which define the resonance model and the interference order (N) of a hexagonal microcavity:

$$\text{WGMs}: \quad R = \frac{hc}{3\sqrt{3}nE}\left[N + \frac{6}{\pi}\arctan\left(\beta\sqrt{3n^2 - 4}\right)\right] \qquad (1)$$

$$\text{FPMs}: \quad d = \frac{Nhc}{2nE} \qquad (2)$$

where, R is the radius of the circumscribing circle of the resonator, n is the refractive index, h is Planck's constant, and c is the speed of light in a vacuum. The factor β is dependent on polarization. For TM polarization, $\beta = 1/n$ and for TE polarization, $\beta = n$.

We performed photoluminescence measurements with detection of unpolarized, TM polarized, and TE polarized signals. Fig. 4(a) shows the typical PL spectra obtained at the position marked by a white cross of the ZnO microtube shown as inset. The origin of the visible emission is mainly attributed to impurities and/or point defects. It can be seen from Fig. 4(a) that a set of resonance peaks coupled to a broad background emission was observed. Taking the refractive index of ZnO ($n \approx 2.0$) for light in the visible spectral range and the radius R of the hexagonal

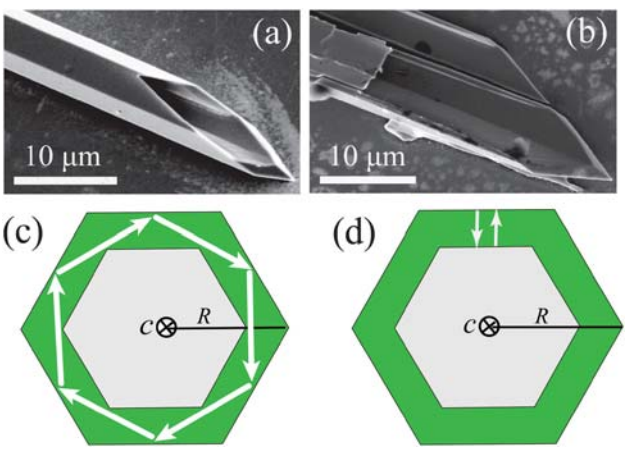

Fig. 3 (a, b) SEM images of a (a) pristine and (b) cracked ZnO microtubes indicating the flat and smooth hexagonal facets of the inner and outer surfaces. Schematics of a microtube with hexagonal cross section, showing light being confined in the (c) WGM resonator and (d) FP resonator due to TIRs as indicated by the arrows.

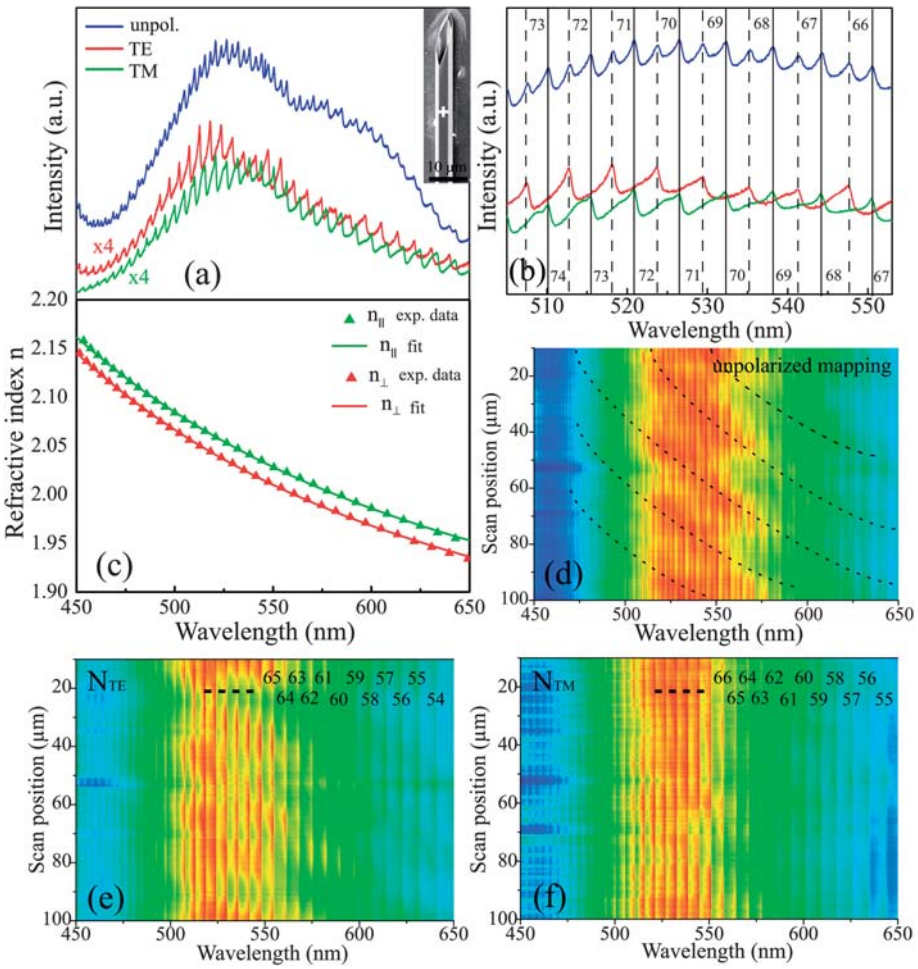

Fig. 4 (a) Photoluminescence spectra for unpolarized (blue curve), TE polarized (red curve) and TM polarized (green curve) light in the visible region from the WGMs. The inset is a SEM image of the ZnO microtube with a side length of 3595 ± 50 nm, and data were collected from the spot marked by a cross. (b) An enlarged view of the resonance peaks between 505 to 553 nm indicating the WGMs formed in the ZnO microtubes with TE and TM polarization configurations. The two sets of integers are the interference order for the corresponding resonant modes. (c) Wavelength dependent refractive indices of the ZnO microtubes for both $n_{\parallel}$ (TM mode) and $n_{\perp}$ (TE mode), as deduced by fitting the scattered refractive indices to Cauchy dispersion functions. (d,e,f) Spatially resolved PL mapping along the microtube *c*-axis with unpolarized, TE, and TM detection, respectively.

cavity (3595 nm) as measured by SEM, we performed an initial calculation, which shows that the photon energy of these peaks fulfils the resonance condition of eqn (1). This effect confirmed that the measured resonance modes are WGMs. Both TE and TM polarized modes are clearly present with similar intensity. The results are different from previous studies in which ZnO WGMs are preferentially TM polarized and the TE modes are weak and broad, or hardly resolved.[1,27] An enlarged view of the resonance peaks between 505 and 553 nm is shown in Fig. 4(b), clearly showing a well-defined WGM resonator for both TE and TM polarization configurations. The vertical solid and dashed lines mark the TM and TE WGM resonant energies, respectively. In addition, it is clearly seen that all the WGM resonance peaks are asymmetric with a long tail at the high energy side of the spectra. We attribute this distinct behavior to the effect of parabolic $E \sim k$ dispersion along the *c*-axis of the microtube.

To further explore the characteristics of the WGM resonator of the ZnO microtube, we carried out identification of the interference order N for the TM and TE modes using the above WGM equation. The refractive indices, $n_{\parallel}$ and $n_{\perp}$, can be obtained from the best fit of the WGM equation, varying N discretely and the radius R within the experimental error. A similar fitting process was also used in the studies of hexagonally shaped ZnO resonators in ref. 27. The obtained scattered wavelength-dependent refractive indices $n_{\parallel}$ and $n_{\perp}$ were fitted by using the Cauchy dispersion formula as follows:

$$n_{\perp} = 1.763 + 6.916 \times 10^4/\lambda^2 + 1.672 \times 10^9/\lambda^4 \quad (3)$$

$$n_{\parallel} = 1.767 + 7.748 \times 10^4/\lambda^2 + 0.513 \times 10^9/\lambda^4 \quad (4)$$

The refractive indices obtained from the above fitting process are shown in Fig. 4(c). It can be seen that the refractive index $n_{\parallel}$ is larger than $n_{\perp}$ at the same wavelength, and both of them decrease with increasing wavelength. The two sets of integers shown in Fig. 4(b) are the interference order for the corresponding resonant modes with the cavity size of $R = 3595$ nm.

To further investigate the cavity qualities and the resonant properties of the synthesized hexagonal microtube cavity, we scanned the excitation beam along the *c*-axis of the microtube

(scanning step of 0.5 μm), while detecting the unpolarized, TE polarized and TM polarized emission. The results are shown in Fig. 4(d)–(f). From the photoluminescence mapping, one can clearly resolve two sets of WGMs with different periodicity. These two sets of WGMs are well separated when we detect the emission in either TE or TM polarization. The straightness and strong WGMs with very narrow linewidth indicate the high quality and uniformity of our microtube cavity. It is expected that the presence of the inner surface in a microtube will lead to mode types that are more complex than those in a microcavity with a single boundary. It is interesting to see that additional resonance modes also exist in our results as shown by the dashed lines in Fig. 4(d). The visible luminescence band is clearly modulated as the excitation laser is scanned along the microtube *c*-axis. The continual shift of the spectral maxima indicates that the size of the corresponding optical cavity should be continuously changing along the microtube *c*-axis. From the SEM images of the perfect (inset in Fig. 4(a)) and the cracked (Fig. S2, ESI†) ZnO microtubes, we can see that the thickness (*d*) of the wall decreases continuously along the *c*-axis of the microtube used in the PL measurement, while the outer radius (*R*) remains uniform. Combining this with the energy spacing of two adjacent modes, one can attribute the additional resonance modes to the Fabry-Pérot (FP)-type cavity modes formed between the inner and outer wall facets. Due to the fact that the reflectance of visible light at the ZnO–air boundary never exceeds 13% at normal incidence conditions regardless of polarization,[8] the FPMs are usually very weak and difficult to observe. It is surprising that the FPMs can be clearly identified in our microtubes.

From the experimental and theoretical analysis, we know that the wall of the microtube functions as the optical microcavity. It must be thick enough to ensure the formation of WGMs or FPMs. However, surprisingly, the resonant modes are also observed in the microtube with thin side walls, as shown in Fig. 5(a). The wall thickness and outer diameter of the microtube are 0.75–0.95 μm and 10.51–11.05 μm, respectively. According to the above analysis, the wall thickness does not fulfil the requirement of WGMs and FPMs formation in the microtube.

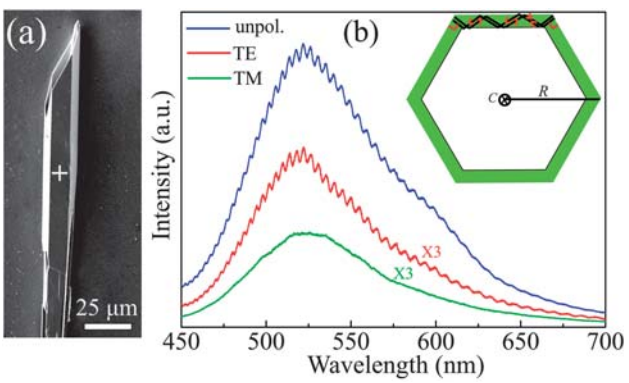

Fig. 5 (a) SEM image of a microtube, and the data in (b) were collected from the region marked by a cross. (b) Unpolarized (blue curve), TE-polarized (red curve) and TM-polarized (green curve) PL spectra in the visible region showing resonator modulations. The inset is a schematic showing the propagation of the light within the microtube walls.

From Fig. 5(b), these resonant modes are preferentially TE polarized and have relatively lower quality factor *Q*, which is different from the WGMs. Taking into account the wall thickness and the outer diameter *R*, we conclude that this type of modulation is attributed to light propagating along the transverse direction of the wall (as shown in Fig. 5(b)) and are similar to the resonant modes in nanobelts.[28] The mode spacing can be calculated by the following equation:

$$\Delta\lambda = \frac{\lambda^2}{2L\left(n - \lambda\frac{dn}{d\lambda}\right)} \quad (5)$$

where L is the effective length of the cavity and n is the refractive index of medium. For the measured microtube, $L = 2R/\sqrt{3} = 12.07$ μm, $n = 2.04$, and $\lambda dn/d\lambda$ is approximately -0.595 (calculated by the above fitted refractive index equation), we obtained the mode spacing of 4.1 nm, which is consistent with the measured value of 4.2 nm. These results show the diversity and complexity of the optical behavior in a microtube cavity. This promises novel applications and greater device versatility.

Conclusion

In summary, we reported the synthesis of ZnO microtubes through a simple oxidation–sublimation process without catalysts, templates, carrier gases or low pressure. SEM and TEM studies show the hexagonal single-crystalline ZnO microtubes have very smooth inner and outer surfaces and highly uniform morphology, and can be used as optical cavities. In addition to WGMs and FPMs, an additional set of modes is observed with different polarization behavior. The effect of the inner facets and the wall thickness on the light modulations is discussed in detail. The refractive indices of the ZnO are determined and the three types of resonant modes are analyzed using a simple plane wave interference model and the Cauchy dispersion function. Our results suggest that ZnO microtube resonators are ideal for the study of resonance mode behavior and the development of novel optical devices.

Acknowledgements

This work is funded by the NSFC 973 projects of China (Grant Nos. 2004CB619004 and 2006CB921506). The Australian authors acknowledge the financial support from the Australian Government Department of Innovation, Industry, Science and Research for funding this collaborative research under the International Science Linkages (China) Program and the Australian Research Council. We are indebted to Professor Chengzhong Yu and Dr Yan Sun for their assistance in SEM and TEM.

References

1 T. Nobis, E. M. Kaidashev, A. Rahm, M. Lorenz and M. Grundmann, *Phys. Rev. Lett.*, 2004, **93**, 103903.
2 F. Qian, Y. Li, S. Gradecak, H.-G. Park, Y. Dong, Y. Ding, Z. L. Wang and C. M. Lieber, *Nat. Mater.*, 2008, **7**, 701.
3 Y. Zhang, H. J. Zhou, S. W. Liu, Z. R. Tian and M. Xiao, *Nano Lett.*, 2009, **9**, 2109.
4 X. Duan, Y. Huang, R. Agarwal and C. M. Lieber, *Nature*, 2003, **421**, 241.

5 Y. S. Zhao, J. J. Xu, A. D. Peng, H. B. Fu, Y. Ma, L. Jiang and J. N. Yao, *Angew. Chem., Int. Ed.*, 2008, **47**, 7301.
6 L. Maleki, A. A. Savchenko, A. B. Matsko and V. S. Ilchenko, *Proc. SPIE*, 2004, **5435**, 178.
7 F. X. Gu, L. Zhang, X. F. Yin and L. M. Tong, *Nano Lett.*, 2008, **8**, 2757.
8 J. Z. Liu, S. Lee, Y. H. Ahn, J. Y. Park, K. H. Koh and K. H. Park, *Appl. Phys. Lett.*, 2008, **92**, 263102.
9 H. X. Dong, Z. H. Chen, L. X. Sun, J. Lu, W. Xie, H. H. Tan, C. Jagadish and X. C. Shen, *Appl. Phys. Lett.*, 2009, **94**, 173115.
10 L. X. Sun, Z. H. Chen, Q. J. Ren, K. Yu, L. H. Bai, W. H. Zhou, H. Xiong, Z. Q. Zhu and X. C. Shen, *Phys. Rev. Lett.*, 2008, **100**, 156403.
11 H. W. Gu and T. M. Swager, *Adv. Mater.*, 2008, **20**, 4433.
12 Y. G. Sun and Y. N. Xia, *Adv. Mater.*, 2004, **16**, 264.
13 S. Iijima, *Nature*, 1991, **354**, 56.
14 L. E. Greene, M. Law, D. H. Tan, M. Montano, J. Goldberger, G. Somorjai and P. D. Yang, *Nano Lett.*, 2005, **5**, 1231.
15 Z. W. Pan, Z. R. Dai and Z. L. Wang, *Science*, 2001, **291**, 1947.
16 X. H. Zhang, Y. Zhang, J. Xu, Z. Wang, X. H. Chen, D. P. Yu, P. Zhang, H. H. Qi and Y. J. Tian, *Appl. Phys. Lett.*, 2005, **87**, 123111.
17 J. Z. Liu, S. Lee, Y. H. Ahn, J. Y. Park, K. H. Koh and K. H. Park, *Appl. Phys. Lett.*, 2008, **92**, 263102.
18 L. Li, H. Q. Yang, G. C. Qi, J. H. Ma, X. L. Xie, H. Zhao and F. Gao, *Chem. Phys. Lett.*, 2008, **455**, 93.
19 P. X. Gao, C. S. Lao, Y. Ding and Z. L. Wang, *Adv. Funct. Mater.*, 2006, **16**, 53.
20 Y. J. Xing, Z. H. Xi, X. D. Zhang, J. H. Song, R. M. Wang, J. Xu, Z. Q. Xue and D. P. Yu, *Solid State Commun.*, 2004, **129**, 671.
21 X. P. Shen, A. H. Yuan, Y. M. Hu, Y. Jiang, Z. Xu and Z. Hu, *Nanotechnology*, 2005, **16**, 2039.
22 Y. Xi, J. H. Song, S. Xu, R. S. Yang, Z. Y. Gao, C. G. Hu and Z. L. Wang, *J. Mater. Chem.*, 2009, **19**, 9260.
23 Y. Sun, G. M. Fuge, N. A. Fox, D. J. Riley and N. R. Ashfold, *Adv. Mater.*, 2005, **17**, 2477.
24 P. X. Gao and Z. L. Wang, *J. Am. Chem. Soc.*, 2003, **125**, 11299.
25 Y. N. Xia, Y. J. Xiong, B. Lim and S. E. Skrabalak, *Angew. Chem., Int. Ed.*, 2009, **48**, 60.
26 J. Wiersig, *Phys. Rev. A: At., Mol., Opt. Phys.*, 2003, **67**, 023807.
27 C. Czekalla, C. Sturm, R. Schmidt-Grund, B. Q. Cao, M. Lorenz and M. Grundmann, *Appl. Phys. Lett.*, 2008, **92**, 241102.
28 M. Law, D. J. Sirbuly, J. C. Johnson, J. Goldberger, R. J. Saykally and P. D. Yang, *Science*, 2004, **305**, 1269.